PHYSICAL REVIEW D

PARTICLES AND FIELDS

THIRD SERIES, VOLUME 27, NUMBER 1 1 JANUARY 1983

Study of A_2 production in the reaction $\pi^- p \to K^0 K^- p$ at 50, 100, and 175 GeV/c

C. Bromberg,* J. O. Dickey,† G. Fox, R. Gomez, W. Kropac,‡ J. Pine, and S. R. Stampke
California Institute of Technology, Pasadena, California 91125

H. Haggerty and E. Malamud
Fermi National Accelerator Laboratory, Batavia, Illinois 60510

R. Abrams, R. Delzenero, F. Lopez, S. Margulies, D. McLeod, and J. Solomon
University of Illinois at Chicago Circle, Chicago, Illinois 60680

A. Dzierba, F. Fredericksen, R. M. Heinz, J. Krider, H. Martin, and D. V. Petersen
Indiana University, Bloomington, Indiana 47405
(Received 29 June 1982)

The reaction $\pi^- p \to K^0 K^- p$ has been measured from 50 to 175 GeV/c. The production characteristics of the A_2 have been analyzed. We find spin and t dependence similar to lower energies, but the cross section falls rapidly with energy. In a Regge description of $\pi^- p \to A_2^- p$ our data imply a rather small Pomeron-exchange component.

I. INTRODUCTION

In recent years several studies have been published of A_2 production in the reaction $\pi^- p \to K^0 K^- p$ at incident momenta up to about 20 GeV/c.[1-5] Over the range studied the energy dependence of the A_2 production cross section $d\sigma/dt$ and the A_2 density-matrix elements are consistent with production of A_2 dominantly via natural-parity exchange. We report here our results of a study of the reaction $\pi^- p \to K^0 K^- p$ at beam momenta of 50, 100, and 175 GeV/c. This was part of an experiment on the Fermilab multiparticle spectrometer involving triggers on several well-defined final-state topologies. The trigger for this reaction selected events with a neutral V (two charged tracks intersecting downstream of the target), one charged track from the target, and at least one recoil hit in the counters surrounding the target. The apparatus, event reconstruction and selection, and the event weighting will be discussed in Sec. II.

We have observed that the reaction $\pi^- p \to K^0 K^- p$ is dominated by A_2 production. We have not found any other statistically significant indications of structure in the $K^0 K^-$ mass spectrum. The Gottfried-Jackson angular distributions in the A_2 region are consistent with those found at lower energies. These distributions and the density-matrix elements are presented in Sec. III, as are the cross sections and a comparison with lower-energy results. Section IV is a summary of our conclusions.

II. APPARATUS AND ANALYSIS

A. Overview of apparatus

The Fermilab multiparticle spectrometer (MPS), shown in Figs. 1 and 2, is located in the M6W beam line. This beam line contained four gas Čerenkov counters which allowed separation of π's, K's, and $\bar{p}$'s in the beam. The MPS itself is designed to measure forward-going charged-particle systems.[6,7] We will describe here only those portions of the system of particular importance to this trigger.

An incident-beam particle was defined by a coincidence between the beam counters *Sa* and *Sb*, and an anticoincidence with the halo veto *Sc*. The beam rate was approximately 7×10^5/sec. A beam interaction was defined for this experiment as an incident beam particle which failed to register in the beam veto counter *Sd*, a 5.08-cm $\times$ 5.08-cm scintillator (2.54 cm $\times$ 2.54 cm for 175-GeV/c data) located 13.3 m downstream of the target and centered on the beam spot. Such an interaction (pretrigger) initiated the check of selective trigger conditions detailed below.

The incident-beam direction was defined by seven proportional-wire-chamber planes, four with 2-mm wire spacing (two horizontal and two vertical) locat-

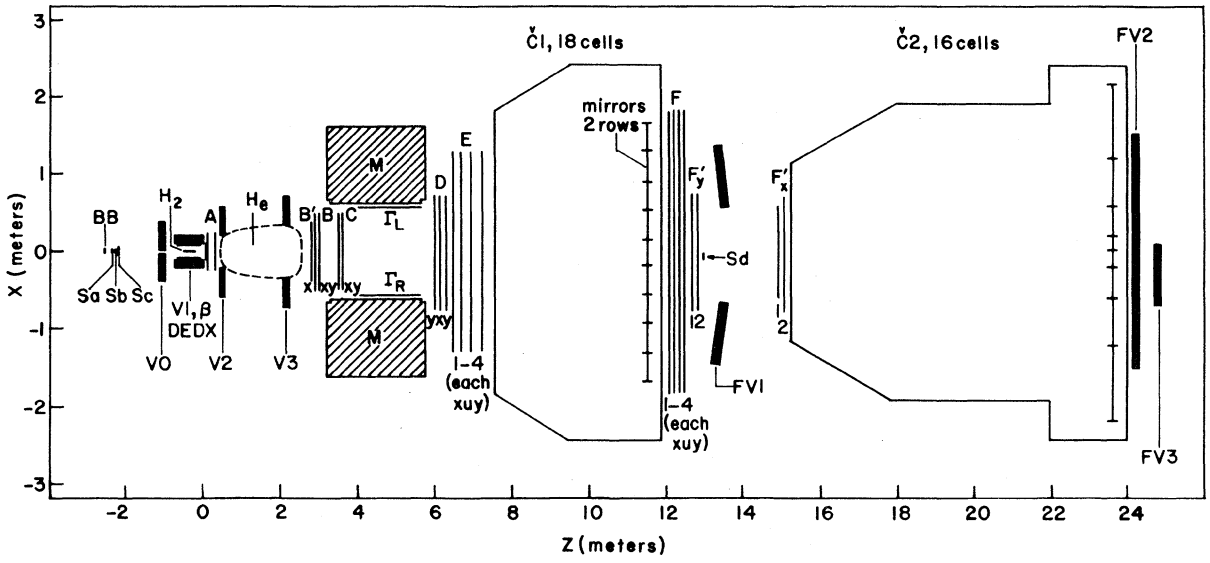

FIG. 1. Multiparticle spectrometer, plan view. *Sa*, *Sb*, *Sc*, *DEDX*, and *Sd* are scintillation counters. *V*0, *V*1, *V*2, and *V*3 are lead-scintillator sandwich veto counters. *BB*, *A*, *B'*, *B*, *C*, *D*, *F*, *β*, and Γ are proportional wire chambers. *E* and *F* are sets of wire spark chambers. Č1 and Č2 are segmented gas Cerenkov counters. *FV*1, *FV*2, and *FV*3 are the forward γ detectors discussed in the text.

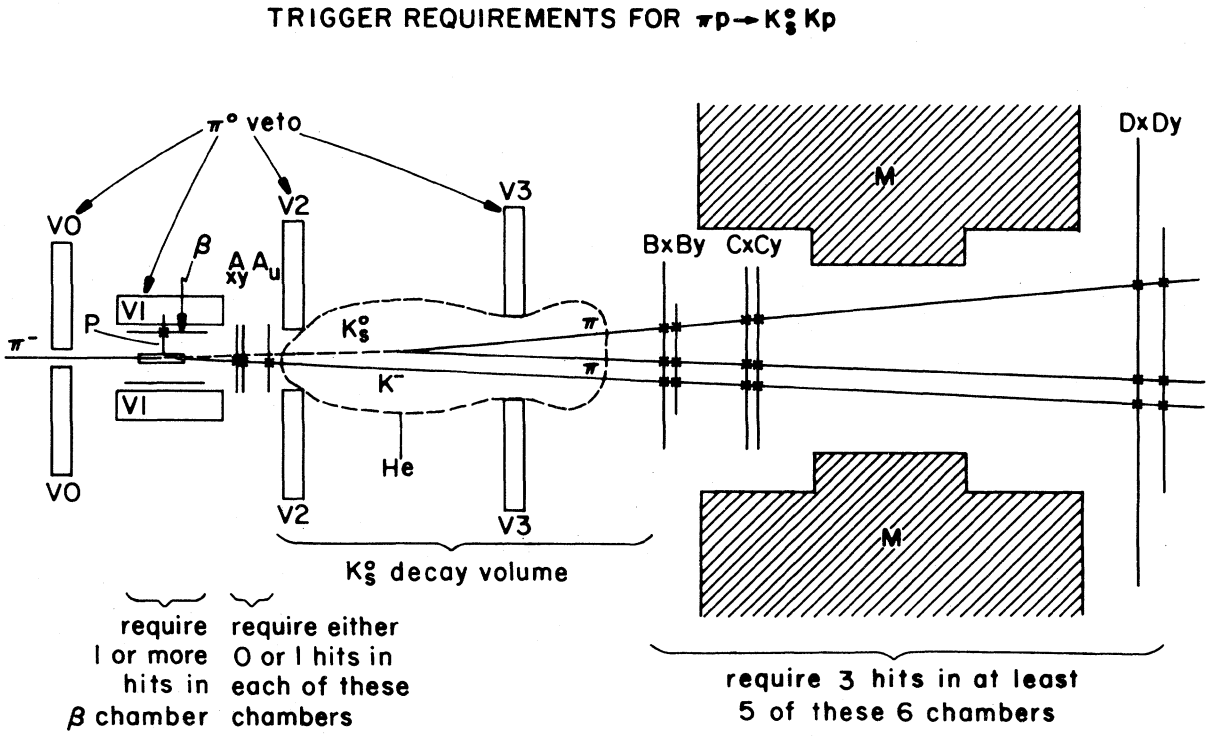

FIG. 2. Multiparticle spectrometer front end, side view, and diagram of trigger requirements.

ed 19.7 m upstream of the target, and three with 1-mm wire spacing (one each of horizontal, vertical, and slant wires) 2.2 m upstream of the target. Target region detectors surrounding a 30.5-cm-long, 2.54-cm-diameter, liquid-hydrogen target detected recoil charged particles and vetoed on the presence of γ's. These consisted of a cylindrical proportional wire chamber β around the target and a set of lead-scintillator shower counters $V0-V3$ surrounding the target except in the beam and forward directions. One of these, $V1$, was a segmented cylindrical counter with 24 azimuthal sections around the chamber. The target-region requirements of our trigger were that (1) the β chamber must detect at least one charged particle, and (2) none of the veto counters, with the exception of segments of $V1$ directly behind β hits, may register a hit.

The momenta and directions of the forward-going charged particles were obtained from a system of proportional wire chambers (PWC's) and wire spark chambers and a large-aperture superconducting magnet. The magnet was operated at a central field strength of 17.8 kG and had an effective length of 1.4 m, imparting a transverse momentum of 0.75 GeV/c. There were three groups of PWC planes upstream of the magnet. The group near the target had six planes with 1-mm wire spacing, three of which, Ax, Ay, and Au, were used in the multiplicity trigger. The other two groups, near the magnet, had a total of five planes, all with 2-mm spacing, four (Bx, By, Cx, and Cy) being used in the trigger. The downstream system consisted of seven PWC planes (D and F' stations) and two sets, twelve planes each (four x planes, four y planes, and four slant planes at 5.7°) of wire spark chambers (E and F stations). Only two of the downstream PWC planes were used in the trigger (Dx and Dy).

The trigger was designed to select events with a single V and one charged track from the main interaction vertex by detecting a change in charged-particle multiplicity from one (near the target) to three (near the magnet). In order to do this the number of hits in each of the trigger planes was counted. The requirement near the target was that there be either zero or one hit in each of the three A chambers. For much of the data the multiplicity increase requirement was that there be exactly three hits in three of the six B, C, and D planes and that one of the two D planes have less than four hits. It was found during the run that this allowed too many spurious triggers which had to be rejected by the event-reconstruction programs. Thus for the balance of the data a stricter requirement was imposed, i.e., that there must be three hits in at least five of the six BCD planes. A helium-filled bag was positioned between the A and B stations to reduce downstream interactions which could produce a false trigger. These trigger requirements are summarized in Fig. 2. The trigger rate was about 6/sec and 3/sec at 100 and 175 GeV/c, respectively.

It was also observed during the early running that events with missing neutrals were even more bothersome than expected. In order to identify and eliminate this background a set of counters was added for the remainder of the data run. These consisted of the Caltech-LBL photon detector,[8] the E260 electron-calorimeter modules,[9] and a set of 20 large scintillator paddles behind a lead wall. Taken together they covered most of the forward direction. Unlike the target region γ-ray detectors $V0-V3$, these were not used in a veto mode, but hits were recorded for use in subsequent analysis.

B. Event reconstruction

The track-finding and event-reconstruction program used on these data, E110 TEARS, has many of its essential features described in two theses.[6,7] Event reconstruction began with the chambers downstream of the magnet by doing a track search independently in the x (11 planes) and y (12 planes) views. The x and y track images were then matched by use of the 5.7° stereo (eight planes) views. The overall efficiency for a spark chamber to have a spark on a given track was, typically, 97%. The corresponding number for a PWC was 95%. Our minimal requirement for a downstream track segment was 15 hits. We have found that these combined to give a downstream track-finding efficiency of 99.5%. Our major sources of track loss were physical effects such as charged-particle decay, multiple scattering, and secondary interactions in the spectrometer material. Once the downstream track images had been found, we attempted to link each of them through the magnetic field to the hit patterns in the upstream chambers. This was done twice for each track: first, using just the chambers (B', B, and C) downstream of the strange-particle decay region for V-track candidates, and second, also using the A chambers for main vertex track candidates.

Reconstruction of V's was accomplished by looping over all oppositely charged pairs of V-track candidates and attempting a vertex fit. The momentum vector of each V candidate with an acceptable

χ^2 and vertex within an enlarged decay volume was used to compute the momentum vector of the parent neutral particle. Event candidates were then formed by a vertex fit using all combinations of neutral trajectory and remaining vertex-track candidates that satisfy the trigger. In the case of multiple event interpretations, the one with the lowest vertex χ^2 was chosen.

C. Event selection

Since a multiplicity-counting trigger is subject to being fooled by a variety of electronic as well as physical background effects, a series of cuts was necessary to go from the initial trigger sample to the final data sample. These are summarized in Table I.

The first three cuts in the table were performed on the data following event reconstruction and eliminated false triggers (due primarily to noise in the chambers) where we were unable to reconstruct an event of the proper form: one negatively charged track from the primary vertex, and one neutral V decaying downstream. Those events whose observed energy was within a rather broad window of the beam energy (± 25 GeV at 100 and 175 GeV/c, ± 12.5 GeV at 50 GeV/c) were written onto a summary tape where only the essential event information was preserved, such as particle trajectories and momenta. The rest of the cuts were performed on this summary tape.

We insisted that the incident particle be tagged as a π by the beam Čerenkov counters. We have studied the response of these counters[6] and found that the efficiencies for properly tagging an incident π at 50, 100, and 175 GeV/c are 99%, 99%, and 96%, respectively. On the other hand, the probabilities of tagging either a K or a $\bar{p}$ as a π are 0.02%, 0.14%, and 0.56% at the three momenta. The beam veto cut is for an instrumental effect. The event, as reconstructed, would have hit the beam veto counter and could not have satisfied the trigger, but appears because of counter inefficiency or spark-chamber memory time. These events were rejected in order to have a well-defined geometrical acceptance.

In Fig. 3 we show the distribution along the beam axis of the main vertex of events at 100 GeV/c surviving the above cuts. It is clear that a large portion of our data is from the material near the first set of PWC's. This is because diffractive (three-track) events occurring in this material would have their tracks unresolved at the first chambers and so satisfy the trigger requirements if a δ ray had been produced in the target to fire the β chamber. We have insisted the main vertex lie between the limits shown. It has been found that this, when combined with the other cuts to be discussed, leaves no observable contamination in the final data sample from events in the downstream peak. We have also insisted that the decay vertex be between the A and

TABLE I. The number of events surviving the various cuts for each setting of the beam momentum.

	50 GeV/c	100 GeV/c	175 GeV/c
Total triggers (no cuts)	17 343	161 345	149 861
Reconstruct one prong and one neutral V	2436	39 823	57 534
Chamber hits satisfy trigger logic	2364	39 148	54 938
Main vertex track negative	2355	38 967	54 289
Energy (loose) (see text)	1526	17 775	13 602
Incident particle tagged as pion	1244	14 067	10 932
All tracks miss Sd	1239	13 867	10 538
Main vertex: $-0.85 < Z_{vtx} < -0.1$ m	622	6968	3827
Decay vertex: $0.35 < Z_{vee} < 2.75$ m	540	6039	3123
Mass of V consistent with K^0: $0.4 < m_{\pi\pi} < 0.6$ GeV/c^2	521	5794	2625
Energy (tight) (see text)	218	1589	1644
Geometrical acceptance	133	1332	1527

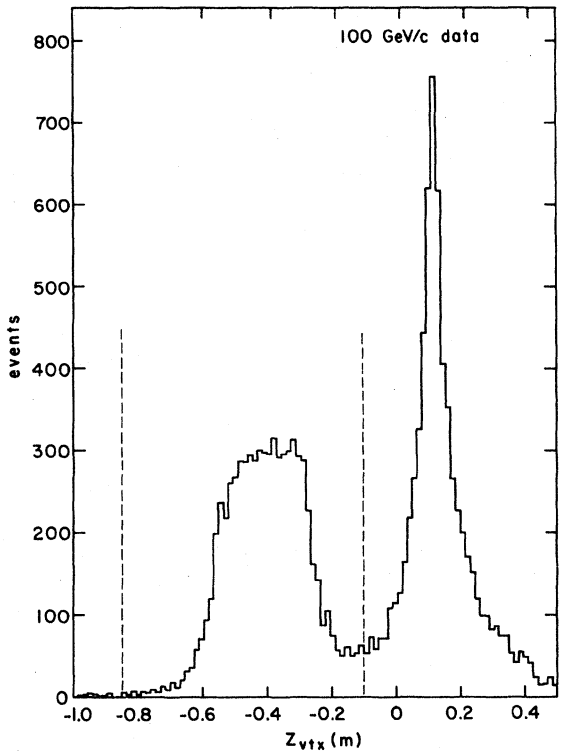

FIG. 3. Primary vertex distribution in beam direction, 100-GeV/c data.

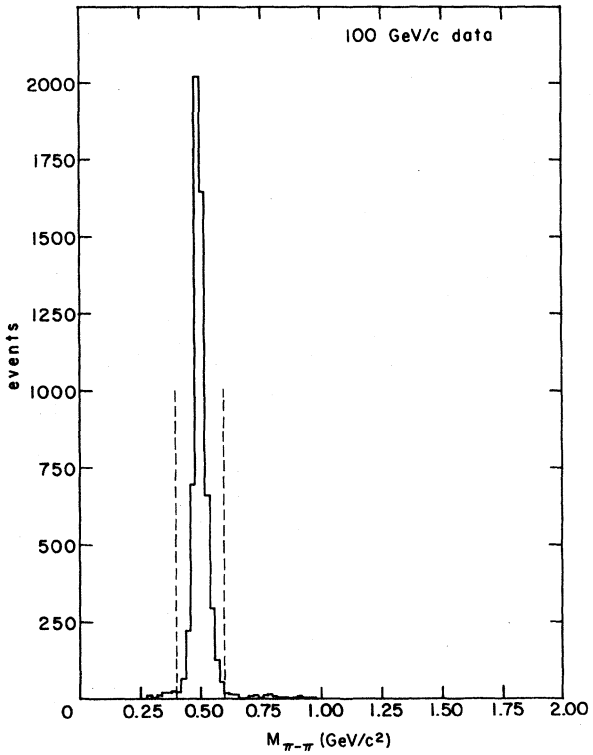

FIG. 4. Effective mass of V for events which pass fiducial volume.

B stations.

The mass spectrum of the neutral decays at 100 GeV/c is shown in Fig. 4 for events which survive the fiducial volume cuts. We have assumed the outgoing particles are pions. We have imposed a cut about the mass of the K^0 of ± 100 MeV. This cut is not strong discrimination against Λ's or $\bar{\Lambda}$'s, since at these secondary-particle energies the apparent effective-mass distribution of misidentified strange baryons is spread across the K^0 mass in a range not much wider than our cut. Thus we are cutting events with severe reconstruction difficulties. However, in the decay of an energetic Λ (or $\bar{\Lambda}$) the outgoing p (or $\bar{p}$) carries most of the momentum, so that if one were to misinterpret it as a K^0 and calculate the polar angle θ_K of the apparent K^0 decay, one would obtain a $\cos\theta_K$ close to -1 ($+1$ for a $\bar{\Lambda}$). That we see no such concentration of events is shown by Fig. 5, the distribution of $\cos\theta_K$ for events at 100 GeV/c which pass all our cuts.

Our final cut was aimed at events in which an additional neutral particle was produced and not observed. Events with our topology could produce one or more neutrals, mainly π^0's, which would be undetected by our veto counters if they were strongly forward. In addition, conservation of strangeness and baryon number requires the production of an additional neutral for most background events which could mimic our topology with particles of different identity. Thus we have cut our events on total visible energy $E_{\rm vis}$ in charged tracks as close to the beam energy as the spectrometer resolution allows. The energy ranges for 50, 100, and 175 GeV/c are, respectively, $48 < E_{\rm vis} < 52$ GeV, $96 < E_{\rm vis} < 104$ GeV, and $161 < E_{\rm vis} < 185$ GeV. Our $E_{\rm vis}$ distribution for the 100-GeV/c data is shown in Fig. 6.

D. Event weighting and background subtraction

The data in this experiment have been weighted event by event to reflect spectrometer efficiency and acceptance and losses from various physical processes and cuts. We further weight each event by the probability that a K^0 of the observed momentum will actually decay within our decay fiducial volume, and by the probability that such an event would be lost through secondary interaction or decay of any of the outgoing particles. We also weight for attenuation of the beam from the beginning of the target to the observed interaction point.

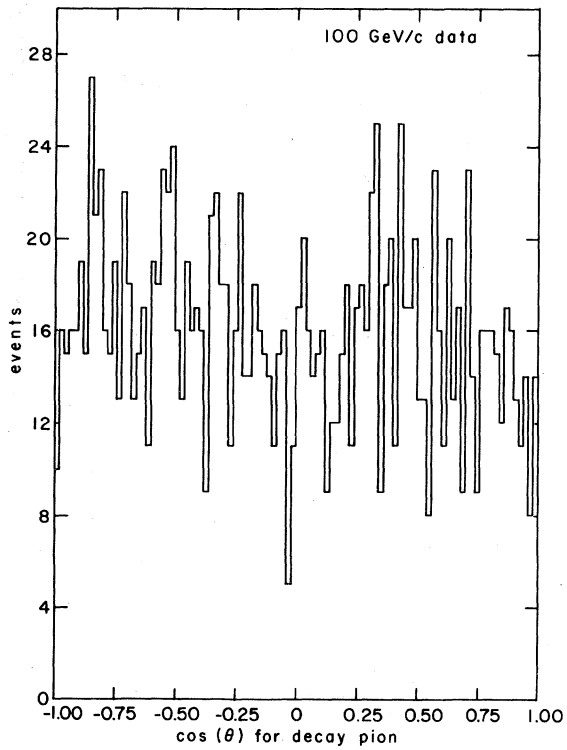

FIG. 5. $\cos\theta$ for π^- from K^0 decay in K^0 rest system, 100-GeV/c data.

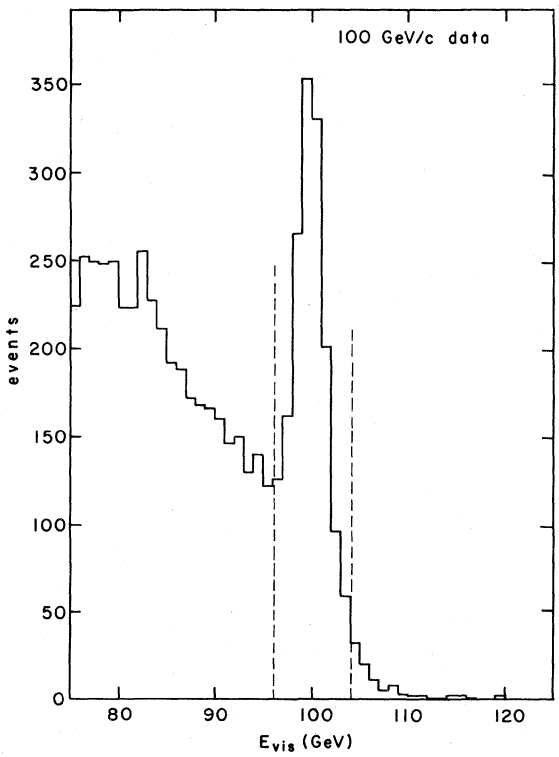

FIG. 6. Total charged-particle energy of events passing fiducial volume and K^0 mass cuts, 100-GeV/c data.

There were three cuts which gave a weight to each event that was a function only of beam momentum. These were the target cut, the K^0 mass cut, and the beam Čerenkov tagging. Their effects are summarized in Table II.

The requirement in our trigger of the recoil proton being detected introduced an inefficiency which was dependent on the momentum transferred to the proton. We have studied this inefficiency by a separate trigger, run simultaneously with the K^0K^-p trigger, which was quite similar except that no recoil was required. The weights we have found for our β-chamber efficiency in various ranges of p_t^2 are listed in Table III. In the lowest p_t^2 ranges the trigger was satisfied not by the recoil proton, but by δ rays. However, we have used such salvaged events because the δ-ray rate was readily and accurately determined. The combined effect of all the above weights, which include everything except geometrical acceptance and reconstruction efficiency, is shown in Fig. 7. The high-weight tail of the distribution is due primarily to the very-low-p_t^2 events.

The geometrical acceptance and reconstruction efficiency were investigated in two ways. Both employed Monte Carlo techniques. In each a set of events was generated and the tracks propagated through the spectrometer. The tracks were checked for whether they would clear the geometrical acceptance. Chamber hits were then generated on the tracks, taking into account the efficiency[7] of each chamber and its measured noise rate for extra hits, and the resultant hit pattern checked for whether the trigger requirements were satisfied. Finally the reconstruction criteria were checked to determine whether the generated event could have been reconstructed.

The first set of events was created from the final data sample. Each event of this sample was used as a starting point and varied in such a way as to keep the dynamical variables of the event unchanged ($M_{K^0K^-}$, t, $\cos\theta_{GJ}$, and ϕ_{GJ}, where $M_{K^0K^-}$ is the effective mass of the kaon pair, t is the four-momentum transfer to the proton, and θ_{GJ} and ϕ_{GJ} are angles of the K^- in the Gottfried-Jackson reference frame). The production point in the target was

TABLE II. Beam-momentum-dependent weights.

Cut	50 GeV/c	100 GeV/c	175 GeV/c
Target	1.000	1.002	1.022
K^0 mass	1.016	1.036	1.09
Beam Čerenkov tag	1.006	1.004	1.03

TABLE III. Weights for recoil-detection efficiency.

p_t^2 range [(GeV/c)^2]	weight
$p_t^2 > 0.14$	1.014
$0.14 > p_t^2 > 0.08$	1.086
$0.08 > p_t^2 > 0.06$	1.104
$0.06 > p_t^2 > 0.04$	1.215
$0.04 > p_t^2 > 0.02$	2.012
$0.02 > p_t^2 > 0.00$	3.106

varied as was the rotation of the event about the beam. The decay time of the K^0 was varied, within the restriction that it must decay inside our fiducial volume, and its decay parameters were picked $(\cos\theta_K, \phi_K)$. The acceptance, trigger, and reconstruction weight for an event was then simply calculated from the fraction of events generated from it which passed the tests of acceptability.

The second set of Monte Carlo events was used only to investigate regions of insensitivity of our apparatus, not for event weighting. It was generated by picking a mass in the A_2 region, where the bulk of our events lie, from a Breit-Wigner distribution, and a t with an exponential distribution consistent with observations at lower energy. However, the Gottfried-Jackson angles were generated to uniformly populate the angular space. We have found no holes in the response of the experiment beyond the capability of the weighting procedures to adequately compensate. The most prominent nonuniformity is a dip at $\phi_{GJ} = 0$ reflecting the presence of the beam veto.

Even when the visible-energy cut is applied to the data there remains a significant background from events with missing neutrals as may be seen from Fig. 6. In order to handle this background the forward neutral-particle detectors were added for the second data run of the experiment (175 GeV/c). Hits in these counters were recorded and compared during analysis with charged-particle trajectories. Events which had a hit in these counters away from the charged particles were tagged as γ-background events. Sections of this system were rendered ineffective by the presence of the charged tracks, and good events could undergo a far-downstream secondary interaction which would produce a separated hit. Thus, account had to be taken of both detector inefficiency and spurious tagging. Figure 8 shows

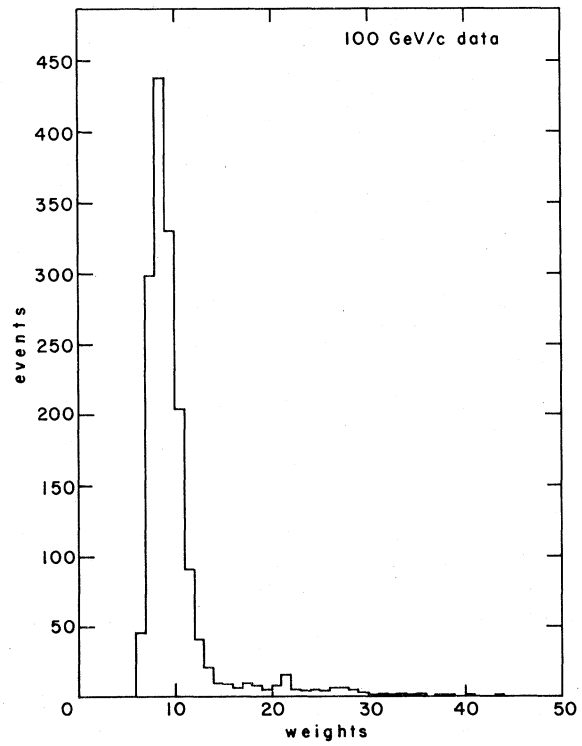

FIG. 7. Distribution of event weights for all effects except acceptance and reconstruction efficiency, 100-GeV/c data.

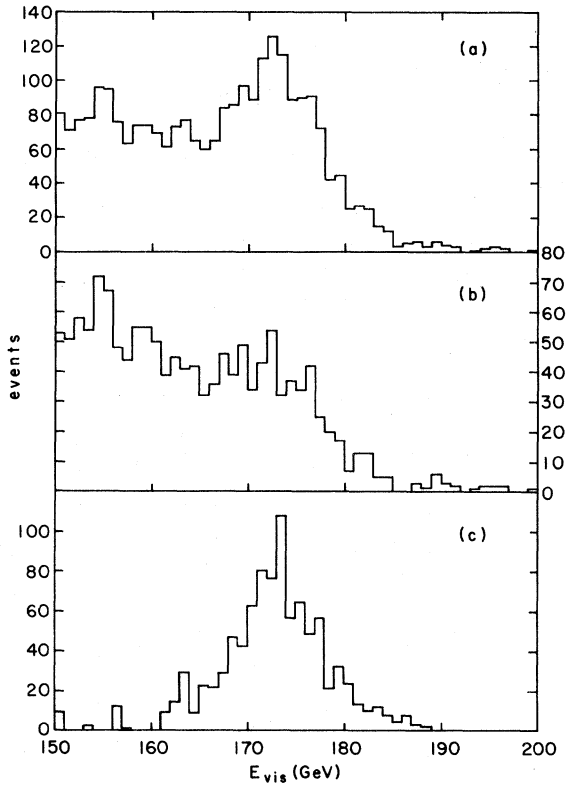

FIG. 8. (a) Total charged-particle energy, 175-GeV/c data. (b) Total charged-particle energy for tagged background events. (c) Total charged-particle energy with background events subtracted.

(a) the observed-energy distribution of events prior to the E_{vis} cut, (b) the energy distribution of the subset of (a) which has a tag for a γ present, and (c) the energy distribution which results from the subtraction of (b) from (a) with adjustments for counter efficiencies.

At our other two beam momenta, where this tagging was unavailable, we were forced to rely on other techniques to estimate the background. This was done by assuming that, except for simple energy scaling, the shape of the background in the distributions of dynamic variables with which we are dealing does not vary significantly from the tagged sample. The relative amounts of background were determined from the observed energy distributions. The tagged 175-GeV/c background events were then scaled and weighted accordingly and used to generate background curves for the dynamic variable distributions at 50 and 100 GeV/c.

III. DISTRIBUTIONS

A. K^0K^- mass distributions

We have analyzed the K^0K^- system, with the above-described cuts and corrections, for production properties and resonant modes. We are insensitive to either K_L^0 decays or neutral decays of the K_S^0, so that all data are multiplied by 2.92 to compensate for these effects. The mass spectrum of our K^0K^- pairs is shown in Fig. 9 for each of our momenta. The only structure evident is the A_2. Observation of the $g(1700)$ has been reported in this spectrum[4]; however our statistics are such that we can make no statement about its presence at the level reported.

The total observed cross sections for $\pi^-p\to K^0K^-p$ are given in Table IV. Also listed is the cross section within the mass cut 1.22 to 1.42 GeV/c^2. Both these are corrected for missing neutrals. We have fit a D-wave Breit-Wigner resonance, using the mass and width from the Particle

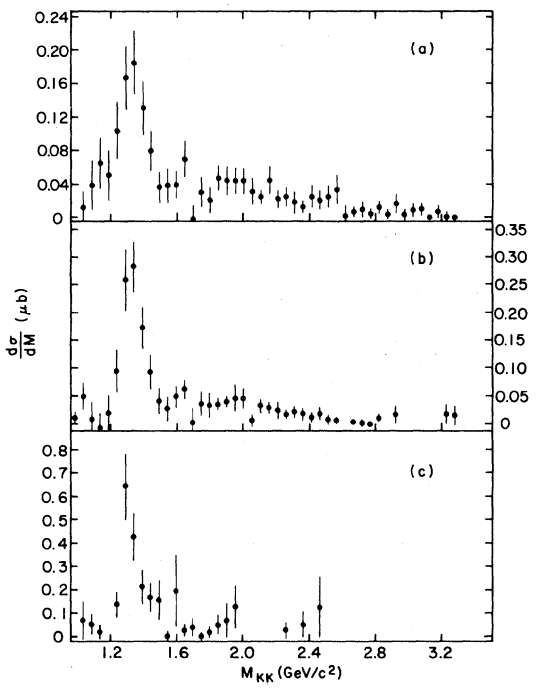

FIG. 9. Effective mass of K^0K^-. (a) 175-GeV/c data. (b) 100-GeV/c data. (c) 50-GeV/c data.

Data Group tables,[10] plus a linear background to the data within the mass range $1.11<m_{KK}<1.52$ GeV/c^2, finding the cross sections for A_2 production times the branching ratio for $A_2^-\to K^0K^-$ which appear in Table IV. We have plotted the $\pi^-p\to A_2^-p\to K^0K^-p$ cross sections as a function of laboratory beam momentum in Fig. 10. The errors shown are statistical. In addition we estimate systematic uncertainties of 6%, 13%, and 18% at 50, 100, and 175 GeV/c, due primarily to estimating background levels.

A falloff of the A_2 production cross section with increasing momentum of $p_{lab}{}^{-0.4}$ has been reported previously.[11] However these data indicate a steeper momentum dependence. If we fit all the points in Fig. 10 to $p_{lab}{}^{-n}$, we obtain $n=0.61\pm0.05$. Using

TABLE IV. Properties of $\pi^-p\to K^0K^-p$. The first line is the total cross section observed in this experiment. The second is the raw cross section within the mass cuts. The third (product of production cross section and branching ratio) and fourth (slope parameter) are obtained from the fits described in the text. All have been corrected for missing-neutral-particle background.

	50 GeV/c	100 GeV/c	175 GeV/c
$\sigma(\pi^-p\to K^0K^-p)$ (μb)	3.02±0.36	1.82±0.07	1.75±0.10
$\sigma(1.22<m_{KK}<1.42$ GeV/$c^2)$ (μb)	1.67±0.20	0.90±0.08	0.63±0.07
$\sigma(A_2)B(A_2^-\to K^0K^-)$ (μb)	2.18±0.39	1.21±0.11	0.65±0.14
b [(GeV/c)$^{-2}$] (A_2 region)	7.5±0.6	8.0±0.5	7.0±0.8

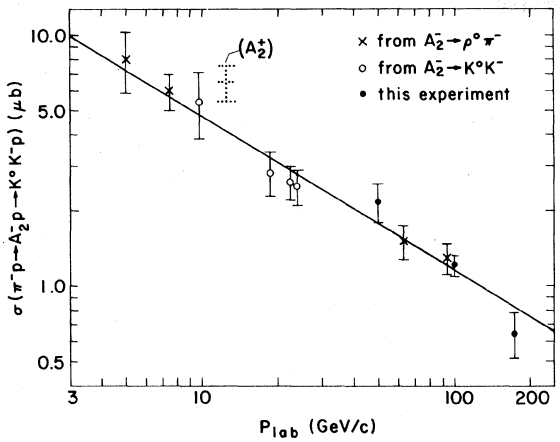

FIG. 10. $\sigma(\pi^- p \to A_2^- p \to K^0 K^- p)$.

only our own points we find $n = 0.94 \pm 0.22$. We have fit the data of Fig. 10 to the Regge form (averaged over four-momentum transfer) $(s/s_0)^{2\alpha - 2}$, obtaining $\alpha = 0.69 \pm 0.03$. Theoretically one expects a mixture of Pomeron and f exchange to dominate. Our data indicate that the Pomeron component is even smaller than anticipated in previous predictions of the cross section.[12] We have run several checks for instrumental effects which might effect the energy dependence of the data. The 50-GeV/c data spanned both data runs, and the two parts of the data are in good agreement. We have also run a rudimentary analysis on the data from our $\pi^- p \to \pi^+ \pi^- \pi^- p$ (diffractive) trigger at 100 and 175 GeV/c. This check was chosen because the reaction has been well studied[11] and the trigger was very similar to that for $K^0 K^- p$. The results show our diffractive cross section to be in agreeement with the measurements from other experiments.

B. t distributions

We have calculated $d\sigma/dt'$ as a function of t' $(\equiv t - t_{\min})$ for the set of events in the A_2 mass region, from 1.22 to 1.42 GeV/c^2. The data have been corrected for both missing-neutral and nonresonant backgrounds, and are shown in Fig. 11. The errors shown are statistical. We have fit these data to the form $d\sigma/dt' = A \,|\, t' \,|\, e^{bt'}$, and find the values for b listed in Table IV. This form was used because it has been found to fit the data reasonably well at low energies, where it gives evidence of helicity-flip dominance. However, the evidence for a downturn of the cross section as t' goes to 0 is not prominent. Indeed at 175 GeV it appears to only be a leveling. At the other two energies there is a marked depletion of events in the lowest bin, but

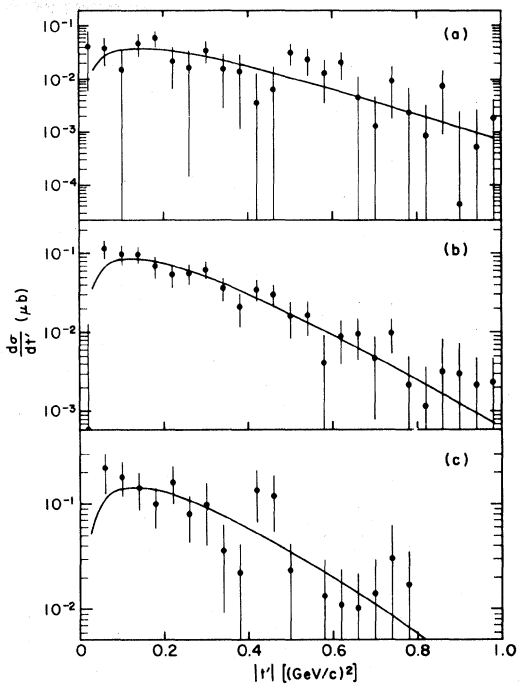

FIG. 11. $d\sigma/dt'$ for $K^0 K^-$ in A_2 mass region. Curves are fits to $A \,|\, t' \,|\, e^{bt'}$. (a) 175-GeV/c data. (b) 100-GeV/c data. (c) 50-GeV/c data.

the other small-t' bins do not turn markedly. Nonetheless, this form gives a fit with reasonable χ^2. Figure 12 is a plot of the parameter b as a function of laboratory momentum. The line is a fit to the form $b = c_1 + c_2 \ln s$ for which we obtain $c_1 = 7.8 \pm 0.7$ and $c_2 = -0.06 \pm .16$.

There is not complete consistency between authors in the form used to fit $d\sigma/dt'$. We have also fit the data to a simple exponential $e^{\beta t'}$ and find at all three momenta that β is consistent with 4.0.

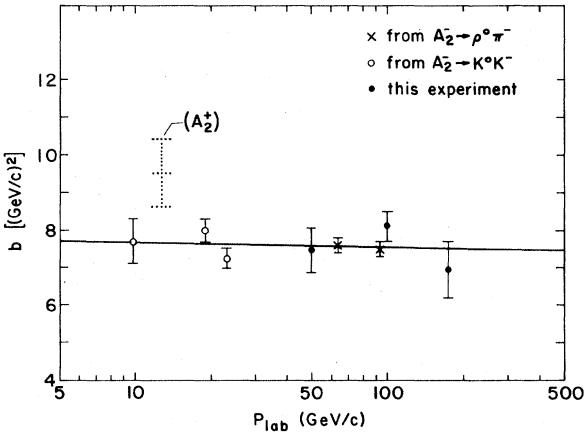

FIG. 12. $d\sigma/dt'$ exponential parameter b as function of p_{lab}. The line is a fit to $b = c_1 + c_2 \ln s$.

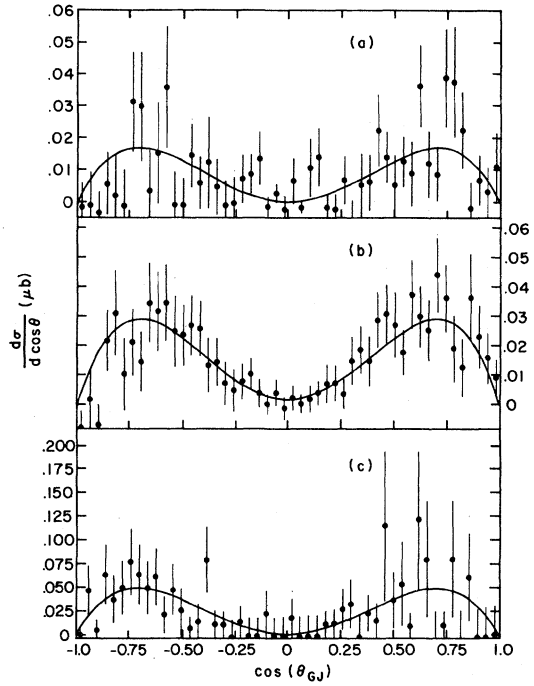

FIG. 13. $\cos\theta_{GJ}$ for events in the A_2 region, nonresonant background subtracted. Curves are fits described in the text.

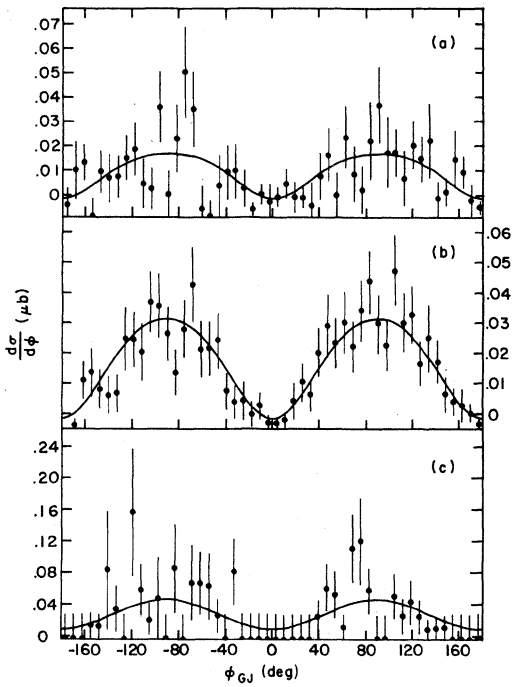

FIG. 14. ϕ_{GJ} for events in A_2 region, nonresonant background subtracted. (a) 175-GeV/c data. (b) 100-GeV/c data. (c) 50-GeV/c data. Curves are fits described in the text.

C. Decay-angular distributions and density-matrix elements

Figures 13 and 14 are the distributions in the Gottfried-Jackson angles, $\cos\theta_{GJ}$ and ϕ_{GJ}, respectively, of the A_2-region events. The same mass cuts and background corrections have been applied as for the $d\sigma/dt'$ plots.

When an A_2 meson with $J^P=2^+$ is formed and then decays into two $J^P=0^-$ mesons, it has the following normalized angular distribution[13] in terms of the density-matrix elements in the Gottfried-Jackson reference frame:

$$I(\theta,\phi)=\frac{15}{16\pi}[\,3\rho_{0,0}(\cos^2\theta-\tfrac{1}{3})^2+4(\rho_{1,1}-\rho_{1,-1}\cos2\phi)\sin^2\theta\cos^2\theta+(\rho_{2,2}+\rho_{2,-2}\cos4\phi)\sin^4\theta$$
$$-4\sqrt{6}\,\mathrm{Re}(\rho_{1,0})(\cos^2\theta-\tfrac{1}{3})\sin\theta\cos\theta\cos\phi+2\sqrt{6}\,\mathrm{Re}(\rho_{2,0})(\cos^2\theta-\tfrac{1}{3})\sin^2\theta\cos2\phi$$
$$-4(\mathrm{Re}(\rho_{2,1})\cos\phi-\mathrm{Re}(\rho_{2,-1})\cos3\phi)\sin^3\theta\cos\theta\,]\,.$$

In view of the statistics of our data, we have attempted to fit only the integrated distributions:

$$I(\theta)=\tfrac{15}{8}[(3\rho_{0,0}-4\rho_{1,1}+\rho_{2,2})\cos^4\theta+2(-\rho_{0,0}+2\rho_{1,1}-\rho_{2,2})\cos^2\theta+(\tfrac{1}{3}\rho_{0,0}+\rho_{2,2})]$$

and

$$I(\phi)=\frac{1}{2\pi}[(\rho_{0,0}+2\rho_{1,1}+2\rho_{2,2})-(2\rho_{1,-1}+\tfrac{2}{3}\sqrt{6}\,\mathrm{Re}(\rho_{2,0}))\cos2\phi+2\rho_{2,-2}\cos4\phi\,]\,,$$

TABLE V. A_2 density-matrix elements.

Matrix elements	50 GeV/c	100 GeV/c	175 GeV/c
$\rho_{0,0}$	0.00±0.06	0.00±0.10	0.00±0.10
$\rho_{1,1}$	0.47±0.05	0.46±0.04	0.49±0.07
$\rho_{2,2}$	0.01±0.02	0.03±0.02	0.00±0.03
$\rho_{1,-1}+\frac{1}{3}\sqrt{6}\rho_{2,0}$	0.33±0.14	0.50±0.03	0.49±0.08
$\rho_{2,-2}$	0.00±0.08	−0.05±0.05	−0.08±0.07

with the constraints (unitarity) that $\rho_{0,0}+2\rho_{1,1}+2\rho_{2,2}=1$ and $|\rho_{1,-1}| < \rho_{1,1}$. In doing this fit we have attempted to remove the nonresonant background by taking the distributions in $\cos\theta_{GJ}$ and ϕ_{GJ} from events outside the A_2 region and subtracting in proportion to the amount of background our fit to the mass spectrum indicated was present. The results are presented in Table V.

Previous experiments on A_2 production have found that, except possibly at very low momentum transfer, both $\rho_{1,1}$ and $\rho_{1,-1}$ are consistent with 0.5 filling the entire unitary bound, and that all the other matrix elements are consistent with 0. We do not have enough events to test the very-low-t region separately, however we find that this condition persists even to our highest energy. Thus it would seem that the A_2 production is mediated entirely by natural-parity exchange.

IV. CONCLUSIONS

We have measured the $\pi^- p \to K^0 K^- p$ reaction with emphasis on the A_2 mass region, across the incident-pion momentum range 50 to 175 GeV/c. We find the A_2 production cross section falls as $p_{\text{lab}}{}^{-0.61}$, indicating that the Pomeron-exchange contribution is very small. We have been able to fit our data in $d\sigma/dt'$ to the exponential form $A\,|t'|\,e^{bt'}$ obtaining $b=7.5\pm0.6$, 8.0 ± 0.5, and 7.0 ± 0.8 (GeV/c)$^{-2}$ at 50, 100, and 175 GeV/c, respectively, in good agreement with previous results. Our angular-distribution analysis indicates that only the density-matrix elements $\rho_{1,1}$ and $\rho_{1,-1}$ are appreciable, being $\frac{1}{2}$, and all others are consistent with zero, indicating natural-parity-exchange dominance.

ACKNOWLEDGMENTS

We would like to gratefully acknowledge the help of the staff of Fermi National Accelerator Laboratory and in particular the meson laboratory crew for the successful operation of this experiment. We also wish to thank the Fermilab computer department where the early, time-consuming, stages of this analysis were done. In addition we express our appreciation of R. Kornblau, M. Lambert, and G. Happoldt for assistance in processing these data. This work was supported in part by the U. S. Department of Energy (Caltech, Fermilab, and Indiana) and by the National Science Foundation (Illinois).

*Present address: Michigan State University, East Lansing, Michigan.
†Present address: Jet Propulsion Laboratory, Pasadena, California.
‡Present address: Hughes Aircraft Corporation, Los Angeles, California.

[1]K. J. Foley *et al.*, Phys. Rev. D 6, 747 (1972).
[2]C. M. Ankenbrandt *et al.*, Phys. Rev. D 8, 2785 (1973).
[3]M. Margulies *et al.*, Phys. Rev. D 14, 667 (1976).
[4]A. D. Martin *et al.*, Phys. Lett. 74B, 417 (1978); Nucl. Phys. B140, 158 (1978).
[5]V. Chabaud *et al.*, Nucl. Phys. B145, 349 (1978).
[6]F. Fredericksen, Ph.D. thesis, Indiana University, 1982 (unpublished).
[7]S. R. Stampke, Ph.D. thesis, California Institute of Technology, 1982 (unpublished).
[8]O. I. Dahl *et al.*, Phys. Rev. Lett. 37, 80 (1976).
[9]H. Haggerty, in Proceedings of the Calorimeter Workshop, Fermilab, 1975 (unpublished).
[10]Particle Data Group, Rev. Mod. Phys. 52, S1 (1980).
[11]C. Daum *et al.*, Nucl. Phys. B182, 269 (1981).
[12]A. C. Irving *et al.*, Nucl. Phys. B149, 101 (1979).
[13]J. D. Jackson, Nuovo Cimento 34, 1644 (1964).